INTERNATIONAL JOURNAL FOR NUMERICAL METHODS IN FLUIDS
Int. J. Numer. Meth. Fluids 2001; **00**:1–00 *Prepared using* fldauth.cls *[Version: 2000/07/27 v1.0]*

Theory and application of 3-D LSKUM based on entropy variables

S. M. Deshpande[1,*], K. Anandhanarayanan[2], C. Praveen[1], V. Ramesh[3]

[1] *CFD Centre, Dept. of Aerospace Engg., Indian Institute of Science, Bangalore.*
[2] *Defence Research and Development Laboratory, Hyderabad.*
[3] *National Aerospace Laboratories, Bangalore.*

SUMMARY

This paper describes the theory and application of a grid-free kinetic upwind scheme known as LSKUM. The basic principle in LSKUM is the determination of derivatives occurring in the conservation laws using the least squares method. The grid-free nature of the scheme is obtained because the least squares method can be used on an arbitrary distribution of nodes, i.e., the nodes need not form a structured/unstructured grid. Copyright © 2001 John Wiley & Sons, Ltd.

KEY WORDS: Euler equations, kinetic scheme, least squares, grid-free, upwinding.

1. Introduction

LSKUM [1, 2] is an acronym for Least Squares Kinetic Upwind Method developed for obtaining numerical solution of Euler equations of gas dynamics and of Navier-Stokes equations of compressible viscous heat conducting fluid. It is a grid-free method capable of operating on an arbitrary distribution of points. Hence it can work on stacked, structured, unstructured, prismatic, Cartesian, background Cartesian overlapping with body fitted meshes and other chimera meshes. It is not essential that the cloud of points be tesselated to form elements such as tetrahedra, prisms, hexahedra and so on. This is one of the attractive features of LSKUM and therefore it is being applied to FAME mesh [3] generated by scientists in DERA, UK. The FAME mesh for a configuration consists of a background Cartesian mesh which progressively becomes finer as body is approached and further it overlaps with several body fitted meshes. Yet another application that is being tried at the CFD Centre, Bangalore, is computation of inviscid supersonic flow around a flight vehicle configuration with deflected fins. All these complicated applications require a preprocessor which operates on the given cloud of points and gives connectivity information for each node. For each P_o, the connectivity $N(P_o)$ is a set of points which are neighbours of P_o. A strict definition of a neighbour is not required, it is enough if we require that a node $P_i \in N(P_o)$ should satisfy $d(P_i, P_o) \leq h$. Here $d(P_i, P_o)$

*Correspondence to: CFD Centre, Department of Aerospace Engineering, Indian Institute of Science, Bangalore-560012, India. Email: suresh@aero.iisc.ernet.in

is the Euclidean distance between P_i and P_o, and h is a characteristic linear dimension of connectivity $N(P_o)$ to be specified by the user.

The 2-D LSKUM has been extensively applied to a number of flow problems which include subsonic, transonic and supersonic flows around airfoils, flow past a biplane, etc. These test cases have been solved using different types of point distributions [4]. Recently Ramesh [4, 15] applied 2-D LSKUM on a variety of point distributions, consisting of simple distributions obtained from structured grids to complex distributions obtained from chimera meshes. The primary purpose of the present paper is to develop and apply 3-D LSKUM to various flow problems and further to study LSKUM based on entropy variables (called q-variables) which were introduced by Deshpande [5] while studying symmetric hyperbolic forms.

2. Basic Theory of Kinetic Schemes

Kinetic schemes for gas dynamics are based on the connection between the Boltzmann equation of kinetic theory and governing equations of continuum fluid dynamics. For a review of kinetic schemes and more references, see Deshpande [6], Godlewski & Raviart [7]. We start with the Boltzmann equation

$$\frac{\partial f}{\partial t} + v_1 \frac{\partial f}{\partial x} + v_2 \frac{\partial f}{\partial y} + v_3 \frac{\partial f}{\partial z} = 0 \tag{1}$$

which is the evolution equation for the velocity distribution function f and the collision term in (1) has been dropped as it is not essential to our analysis here. The velocity distribution function $f = f(t, x, y, z, v_1, v_2, v_3)$ is a function of time, spatial coordinates and the three components of molecular velocity. We need the additional variable I (called internal energy variable) for enforcing a specified ratio γ of specific heats. The velocity distribution function then becomes

$$f = f(t, \vec{x}, \vec{v}, I) \tag{2}$$

The Maxwellian distribution F which is of interest to us here is defined by

$$F = \frac{\rho}{I_o} \left(\frac{\beta}{\pi} \right)^{3/2} \exp\left(-\beta |\vec{v} - \vec{u}|^2 - \frac{I}{I_o} \right) \tag{3}$$

Various symbols are defined by, $\beta = 1/(2RT)$, R = Gas constant per unit mass, T = absolute temperature, I_o = internal energy due to non-translational degrees of freedom, ρ = mass density, $\vec{v}$ = molecular or particle velocity and $\vec{u}$ = fluid velocity. It is a well known fact of the kinetic theory of gases that suitable moments of (1) give the Euler equations of gas dynamics when f = Maxwellian distribution, F. The required moment function vector is

$$\Psi = \begin{bmatrix} 1 \\ v_1 \\ v_2 \\ v_3 \\ I + \dfrac{|\vec{v}|^2}{2} \end{bmatrix} \tag{4}$$

and we define moments of F by

$$(\Psi, F) = \int_{\mathbb{R}^3 \times \mathbb{R}^+} (\Psi F) \mathrm{d}\vec{v} \mathrm{d}I \tag{5}$$

It can be easily shown that the conserved vector U occurring in Euler equations is related to F by

$$U = (\Psi, F) = \begin{bmatrix} \rho \\ \rho u_1 \\ \rho u_2 \\ \rho u_3 \\ e \end{bmatrix} \tag{6}$$

Here e is the total energy per unit volume and is given by

$$e = \frac{p}{\gamma - 1} + \frac{1}{2}\rho |\vec{u}|^2 \tag{7}$$

Similarly, the flux vector $G = (GX, GY, GZ)$ is given by

$$GX = (v_1 \Psi, F) = \begin{bmatrix} \rho u_1 \\ \rho u_1^2 + p \\ \rho u_1 u_2 \\ \rho u_1 u_3 \\ (e + p) u_1 \end{bmatrix} \tag{8}$$

$$GY = (v_2 \Psi, F) = \begin{bmatrix} \rho u_2 \\ \rho u_1 u_2 \\ \rho u_2^2 + p \\ \rho u_2 u_3 \\ (e + p) u_2 \end{bmatrix} \tag{9}$$

$$GZ = (v_3 \Psi, F) = \begin{bmatrix} \rho u_3 \\ \rho u_1 u_3 \\ \rho u_2 u_3 \\ \rho u_3^2 + p \\ (e + p) u_3 \end{bmatrix} \tag{10}$$

The Euler equations

$$\frac{\partial U}{\partial t} + \frac{\partial}{\partial x}(GX) + \frac{\partial}{\partial y}(GY) + \frac{\partial}{\partial z}(GZ) = 0 \tag{11}$$

therefore can be cast in the form

$$\left(\Psi, \frac{\partial F}{\partial t} + v_1 \frac{\partial F}{\partial x} + v_2 \frac{\partial F}{\partial y} + v_3 \frac{\partial F}{\partial z} \right) = 0 \tag{12}$$

This compact form is the basis of most of the kinetic numerical methods. For example, the Kinetic Flux Vector Split (KFVS) Euler equations [8, 9],

$$\begin{aligned} \frac{\partial U}{\partial t} + \frac{\partial}{\partial x}(GX^+) + \frac{\partial}{\partial x}(GX^-) + \frac{\partial}{\partial y}(GY^+) + \frac{\partial}{\partial y}(GY^-) & \\ + \frac{\partial}{\partial z}(GZ^+) + \frac{\partial}{\partial z}(GZ^-) &= 0 \end{aligned} \tag{13}$$

are obtained from (12) by splitting the velocity components as,

$$\left(\Psi, \frac{\partial F}{\partial t} + \frac{v_1 + |v_1|}{2}\frac{\partial F}{\partial x} + \frac{v_1 - |v_1|}{2}\frac{\partial F}{\partial x} + \frac{v_2 + |v_2|}{2}\frac{\partial F}{\partial y} + \frac{v_2 - |v_2|}{2}\frac{\partial F}{\partial y} + \frac{v_3 + |v_3|}{2}\frac{\partial F}{\partial z} + \frac{v_3 - |v_3|}{2}\frac{\partial F}{\partial z}\right) = 0 \quad (14)$$

The KFVS fluxes [8, 9] are given by

$$GX^{\pm} = \left(\frac{v_1 \pm |v_1|}{2}\Psi, F\right), \quad GY^{\pm} = \left(\frac{v_2 \pm |v_2|}{2}\Psi, F\right), \quad GZ^{\pm} = \left(\frac{v_3 \pm |v_3|}{2}\Psi, F\right) \quad (15)$$

The KFVS Euler equations (13) are the basis of cell-centered KFVS-based finite volume Euler codes developed at DRDL, Hyderabad [10, 11].

3. Theory of LSKUM

At the heart of the LSKUM is the least squares formulae for determining the derivatives F_{xo}, F_{yo}, F_{zo} at a node P_o in terms of the data at all $P_i \in N(P_o)$. For P_i we can write

$$F_i = F_o + \Delta x_i F_{xo} + \Delta y_i F_{yo} + \Delta z_i F_{zo} + HOT \quad (16)$$

where HOT = higher order terms in Taylor expansion around node P_o. We can form least squares norm

$$E = \sum_{i \in N(P_o)} w_i (\Delta F_i - \Delta x_i F_{xo} - \Delta y_i F_{yo} - \Delta z_i F_{zo})^2 \quad (17)$$

where w_i are suitable weight functions. The derivatives F_{xo}, F_{yo}, F_{zo} can be obtained by solving the linear algebraic equations

$$\frac{\partial E}{\partial F_{xo}} = \frac{\partial E}{\partial F_{yo}} = \frac{\partial E}{\partial F_{zo}} = 0 \quad (18)$$

The first order accurate least squares formulae for the derivatives are given by

$$\begin{bmatrix} F_{xo}^{(1)} \\ F_{yo}^{(1)} \\ F_{zo}^{(1)} \end{bmatrix} = (LS) \begin{bmatrix} \sum w_i \Delta F_i \Delta x_i \\ \sum w_i \Delta F_i \Delta y_i \\ \sum w_i \Delta F_i \Delta z_i \end{bmatrix} \quad (19)$$

where $\Delta F_i = F_i - F_o$, and $\Delta x_i = x_i - x_o$, $\Delta y_i = y_i - y_o$, $\Delta z_i = z_i - z_o$, and LS is the least squares matrix defined by

$$LS = [A_n^T A_n]^{-1} \quad (20)$$

Here A_n^T is a $3 \times n$ matrix given by

$$A_n^T = \begin{bmatrix} \sqrt{w_1}\Delta x_1 & \sqrt{w_2}\Delta x_2 & ..... & \sqrt{w_n}\Delta x_n \\ \sqrt{w_1}\Delta y_1 & \sqrt{w_2}\Delta y_2 & ..... & \sqrt{w_n}\Delta y_n \\ \sqrt{w_1}\Delta z_1 & \sqrt{w_2}\Delta z_2 & ..... & \sqrt{w_n}\Delta z_n \end{bmatrix} \quad (21)$$

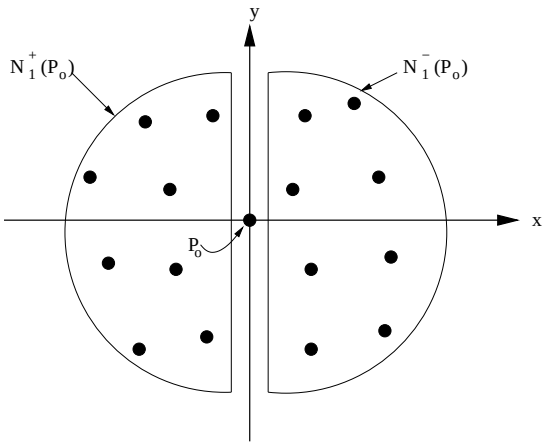

Figure 1. x-split stencil definition for LSKUM; refer equation (23).

and n is the number of points in $N(P_o)$ excluding P_o. The weights w_i can be chosen to make the derivatives local. For example, we can choose

$$w_i = \frac{1}{[d(P_i, P_o)]^p}, \quad P_i \in N(P_o) \tag{22}$$

with p a positive number. A value of $p > 0$ weighs nearby points more than those farther away from P_o. It has been found by Ghosh[1] that $p = 6$ gives the most accurate estimate of the derivative. It is also possible to choose other values of $p < 6$ to change relative weighting. The residue fall has been found to depend on p [1]. The choice $w_i = 1$, the case of uniform weights, has been found to give more rapid residue fall and further it has been shown to have larger numerical dissipation than for $p = 6$ case [1].

We next explain how the least squares formula (19) is used in LSKUM. For this purpose, we split the connectivity (or stencil) $N(P_o)$ of P_o along each of the three coordinate axes. For example, the x-split stencils are denoted by

$$\left.\begin{aligned} N_1^+(P_o) &= [P_i \in N(P_o) : x(P_i) \leq x(P_o)] \\ N_1^-(P_o) &= [P_i \in N(P_o) : x(P_i) \geq x(P_o)] \end{aligned}\right\} \tag{23}$$

These stencils are shown in figure (1), where for simplicity, we have shown splitting in two dimensions only. Note that the exact solution of (1) is given by

$$F(t + \Delta t, x_o, y_o, z_o) = F(t, x_o - v_1\Delta t, y_o - v_2\Delta t, z_o - v_3\Delta t) \tag{24}$$

This indicates that the propagation of information from any node P_i (contributing node) to the receiving node P_o depends upon the location of P_i relative to P_o and the signs of v_1, v_2, v_3. If $v_1 > 0$ then the node P_i will influence the solution at P_o provided P_i lies to the left of P_o, i.e., if $P_i \in N_1^+(P_o)$. Similarly it follows that P_i will influence the solution at P_o for $v_1 < 0$ if $P_i \in N_1^-(P_o)$. This property called the signal propagation property needs to be taken into

account while developing an upwind scheme. Consider for example the term

$$\frac{v_1 + |v_1|}{2}\frac{\partial F}{\partial x}$$

of equation (14). The molecular velocity term multiplying the derivative is always non-negative and hence the derivative should be evaluated using information from $N_1^+(P_o)$. This splitting based on the molecular velocity makes sense because it is molecular motion which carries information in the form of mass, momentum and energy transfer. It is also analogous to using backward difference for convective terms in the advection equation when the advection velocity is positive. The other terms in equation (14) are evaluated in a similar way. After taking $\Psi-$moments of the discretized Boltzmann equation, we obtain the discretized split Euler equations

$$\begin{aligned}\frac{\partial U_o}{\partial t} + \left(\frac{\partial}{\partial x}(GX^+)\right)_{N_1^+(P_o)} + \left(\frac{\partial}{\partial x}(GX^-)\right)_{N_1^-(P_o)} + \left(\frac{\partial}{\partial y}(GY^+)\right)_{N_2^+(P_o)} \\ + \left(\frac{\partial}{\partial y}(GY^-)\right)_{N_2^-(P_o)} + \left(\frac{\partial}{\partial z}(GZ^+)\right)_{N_3^+(P_o)} + \left(\frac{\partial}{\partial z}(GZ^-)\right)_{N_3^-(P_o)} &= 0 \end{aligned} \quad (25)$$

The subscripts in the above equation indicate the appropriate stencil used in the least squares formula to be used for the space derivative inside the brackets. We remark that the Boltzmann equation is used only at the level of formulating the LSKUM and it is equation (25) that we actually solve. Equation (25) can be integrated in time using standard time marching schemes.

4. Defect Correction and q-LSKUM

The extension of LSKUM to second order accuracy is achieved through defect correction [12], which is a method of obtaining second order accurate estimate of the derivatives. We define $\Delta\tilde{F}_i = \tilde{F}_i - \tilde{F}_o$ where

$$\left.\begin{aligned}\tilde{F}_i &= F_i - \frac{1}{2}(\Delta x_i F_{xi}^{(1)} + \Delta y_i F_{yi}^{(1)} + \Delta z_i F_{zi}^{(1)}) \\ \tilde{F}_o &= F_o - \frac{1}{2}(\Delta x_i F_{xo}^{(1)} + \Delta y_i F_{yo}^{(1)} + \Delta z_i F_{zo}^{(1)})\end{aligned}\right\} \quad (26)$$

Replacing ΔF_i with $\Delta\tilde{F}_i$ in equation (19), we obtain the second order accurate estimate for the derivatives

$$\begin{bmatrix} F_{xo}^{(2)} \\ F_{yo}^{(2)} \\ F_{zo}^{(2)} \end{bmatrix} = (LS) \begin{bmatrix} \sum w_i \Delta\tilde{F}_i \Delta x_i \\ \sum w_i \Delta\tilde{F}_i \Delta y_i \\ \sum w_i \Delta\tilde{F}_i \Delta z_i \end{bmatrix} \quad (27)$$

The second order LSKUM is discussed in detail in [12]. Strictly speaking sub-iterations are required to achieve formally second order accuracy. In steady state this will automatically happen when residue saturates. In other cases, a few sub-iterations may be required.

The basic motivation for developing q-LSKUM was the following. Since F is a non-negative velocity distribution function, ΔF_i is the difference between two non-negative Maxwellians.

But $\tilde{F}_i$, $\tilde{F}_o$ may not be non-negative distributions, much less Maxwellians. The q-LSKUM was developed with this fact in mind and we describe it next starting with the q-variables.

The q-variables were introduced by Deshpande [5, 12] while studying the symmetric hyperbolic form of Euler equations. When we make the transformation from U to q, the Euler equations (11) are transformed into the symmetric hyperbolic form

$$P\frac{\partial q}{\partial t} + B_1\frac{\partial q}{\partial x} + B_2\frac{\partial q}{\partial y} + B_3\frac{\partial q}{\partial z} = 0 \tag{28}$$

where P is a 5×5 symmetric positive definite matrix and the B_i are 5×5 symmetric matrices. These q-variables are given by

$$q = \left[\ \ln\rho + \frac{\ln\beta}{\gamma-1} - \beta|\vec{u}|^2, \quad 2\beta u_1, \quad 2\beta u_2, \quad 2\beta u_3, \quad -2\beta\ \right]^T \tag{29}$$

A Maxwellian F is uniquely known in terms of q variables and we denote this Maxwellian by $F(q)$. The q-variables are also called *entropy* variables because they are closely related to the Boltzmann entropy function H [5], through the relation

$$q = \frac{\partial H}{\partial U} \tag{30}$$

In q-LSKUM, the defect correction step of second order LSKUM is modified so as to obtain positive velocity distributions. Consider two Maxwellians, $\tilde{F}_i = F(\tilde{q}_i)$ and $\tilde{F}_o = F(\tilde{q}_o)$, corresponding to the modified entropy variables $\tilde{q}_i$, $\tilde{q}_o$, which are defined as

$$\left.\begin{aligned}\tilde{q}_i &= q_i - \frac{1}{2}(\Delta x_i q_{xi}^{(1)} + \Delta y_i q_{yi}^{(1)} + \Delta z_i q_{zi}^{(1)})\\ \tilde{q}_o &= q_o - \frac{1}{2}(\Delta x_i q_{xo}^{(1)} + \Delta y_i q_{yo}^{(1)} + \Delta z_i q_{zo}^{(1)})\end{aligned}\right\} \tag{31}$$

The equations for $\tilde{q}_i$, $\tilde{q}_o$ are very similar to equations (26). Using limiters for the q-derivatives, we can ensure the positivity of temperature and hence of $p(\tilde{q})$ and consequently we will always get positive velocity distributions. The modified Maxwellians $\tilde{F}_i$, $\tilde{F}_o$ are then substituted in equation (27) for getting formally second order accurate estimates $F_{xo}^{(2)}$, $F_{yo}^{(2)}$, $F_{zo}^{(2)}$. Thus the least squares formulae for first order and second order LSKUM have the same structure, the only difference being the use of modified Maxwellians. It is therefore expected that the second order q-LSKUM might inherit good properties of first order LSKUM such as robustness, smoothness of contours, positivity of density and pressure, and better convergence characteristics.

5. Wall Boundary Condition

Next, we describe the implementation of the boundary condition in LSKUM. The wall boundary condition for inviscid flow is the zero normal velocity condition, $\vec{u}\cdot\vec{n} = 0$ called flow tangency condition. This is implemented in LSKUM using the specular reflection model of kinetic theory of gases. Consider a coordinate system in which the z-axis is along the normal to the wall at a wall boundary point w as shown in figure (2). If (v_1, v_2, v_3) with $v_3 < 0$, is

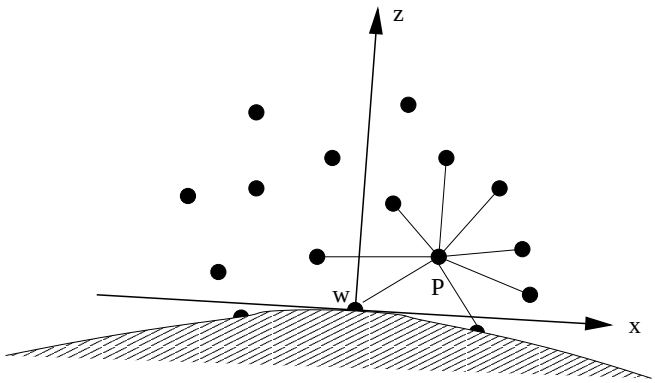

Figure 2. Definition sketch for solid wall points.

the velocity of a molecule before collision with the wall, then its velocity after collision is $(v_1, v_2, -v_3)$. Thus the velocity distribution of reflected molecules is obtained from that of the incident molecules by changing the sign of v_3. The update equation for the incident distribution at a wall point w is

$$F_I^{n+1} = F_w^n - \Delta t \left[\frac{v_1 + |v_1|}{2} \frac{\partial F}{\partial x} + \frac{v_1 - |v_1|}{2} \frac{\partial F}{\partial x} + \frac{v_2 + |v_2|}{2} \frac{\partial F}{\partial y} + \frac{v_2 - |v_2|}{2} \frac{\partial F}{\partial y} + v_3 \frac{\partial F}{\partial z} \right], \qquad v_3 \leq 0 \tag{32}$$

and the corresponding reflected distribution is given by

$$F_R^{n+1}(v_1, v_2, v_3) = F_I^{n+1}(v_1, v_2, -v_3), \quad v_3 \geq 0 \tag{33}$$

The update for U_w can be written as

$$U_w^{n+1} = \int_{v_3 \leq 0} \Psi F_I^{n+1} \mathrm{d}\vec{v}\mathrm{d}I + \int_{v_3 \geq 0} \Psi F_R^{n+1} \mathrm{d}\vec{v}\mathrm{d}I \tag{34}$$

We see from equation (32) that the connectivity of wall point w used for evaluating the derivatives should contain only those points P_i for which $z_i \geq z_w$, and the $\Psi-$moments in (34) lead to different split fluxes (called quadrant split fluxes) which are given elsewhere [13]. The crucial fact here is that we cannot implement the defect correction step of second order LSKUM at a point like P, as shown in figure (2), which is very close to the wall. If $w \in N(P)$, then we need to evaluate the first order estimate of $\partial(GZ^+)/\partial z$ at w, but it may happen that there are not enough points in $N_3^+(w)$. In that case we have to resort to only first order treatment for near-wall points. This will definitely affect the accuracy of the solutions.

On the other hand, the q-LSKUM is second order accurate at all the points, since it does not split the connectivity during the defect correction step for q-variables. Hence even at a point like P in figure (2), there is no problem in obtaining the q-derivatives at w since we are using the full stencil. The stencil is split only while evaluating the split flux derivatives. Similar considerations also apply to the outer boundary condition [14]. We have obtained a dramatic improvement in the solution due to this complete second order treatment.

6. Results and Discussions

The 3-D LSKUM has been applied to various standard test cases. The first result we discuss here is the simulation of an intense blast wave in air [13, 15]. The computational domain is a cube of size $81m \times 81m \times 81m$, and a Cartesian grid of 81^3 points has been used. The test conditions chosen correspond to the Mexico explosion (1945) [16] for which exact solution is available due to Taylor [17]. We assume that the entire energy released in the explosion is initially concentrated in a cubical core of size $10m \times 10m \times 10m$. The initial temperature of this core is estimated to be $8.1 \times 10^7 K$ and the ambient temperature is taken to be $298K$. The ratio of specific heats γ is assumed to be constant. Figure (3) shows the pressure contours at $t = 0.8$ *milliseconds* in the center plane and figure (4) shows the comparison of the shock location at different time instants, with the experiment and the theory of Taylor. It can be observed from the pressure contours that the spherical symmetry of the blast wave is perfectly captured even on a rectangular mesh. This feature of LSKUM is not only due to its robustness but also due to the fact that the solution at a point P depends on the data of all surrounding points in $N(P)$ thus making it almost direction independent.

The q-LSKUM code has been applied to the case of supersonic flow past a hemisphere at $M_\infty = 2$ and $\alpha = 0^o$. The computations were done on grids of size 21^3, 41^3 and 61^3. The residue fall and pressure distribution along the centreline and body are shown in figure (5). Figure (6) shows the pressure and Mach contours obtained on 61^3 grid. For this problem, the stagnation pressure on the body is exactly known and hence it is possible to assess the accuracy of q-LSKUM. Table (1) shows (p_o/p_∞) and (T_o/T_∞) obtained on different grids.

$(p_o/p_\infty)_{exact} = 5.641$, $(T_o/T_\infty)_{exact} = 1.80$

Grid Size	p_o/p_∞	% error	T_o/T_∞	% error
$31 \times 31 \times 31$	5.578	1.109	1.824	1.352
$41 \times 41 \times 41$	5.600	0.729	1.821	1.189
$61 \times 61 \times 61$	5.621	0.360	1.812	0.667

Table I. Analysis of accuracy for flow over a hemisphere, $M_\infty = 2$, $\alpha = 0^o$.

The q-LSKUM used in this study is formally second order accurate and hence it is reasonable to assume that

$$p_o(N) = p_{oe} + \frac{A_1}{N^2} + \frac{A_2}{N^3} + \ldots\ldots$$

where N = total number of grid points and p_{oe} = exact stagnation pressure on the body. We can use Richardson's extrapolation technique to eliminate A_1 and A_2 and determine p_o presumably to higher order of accuracy. Using the 41^3 and 61^3 grids the extrapolated values of (p_o/p_∞) and (T_o/T_∞) are 5.638 and 1.804, giving % errors as 0.055 and 0.237. Using all the three grids, we can do Richardson extrapolation again to obtain even more accurate values. We then get $(p_o/p_\infty) = 5.643$ and $(T_o/T_\infty) = 1.797$ giving % errors of 0.040 and 0.174 respectively.

The next problem solved using q-LSKUM code is the computation of supersonic flow over the Scout vehicle [18] configuration at $M_\infty = 4.65$ and $\alpha = 8^o$. Experimental measurements of C_p at various x-locations are available for this configuration. Figure (7) shows the pressure distribution along the body for windward and leeward sides of the vehicle and the residue fall. Measured value of C_p are also shown in this figure for comparison. Figure (8) shows a

section of the grid used and Mach contours. The aerodynamic coefficients obtained for this configuration agree very well with the experimental values and are shown in table (2).

Coefficient	q-LSKUM	Experiment	% error
Normal Force	0.963	0.928	3.77
Pitching Moment	2.732	2.627	3.99

Table II. Aerodynamic coefficients for flow over Scout vehicle configuration obtained using q-LSKUM on a grid of $81 \times 33 \times 21$ points at $M_\infty = 4.65$ and $\alpha = 8^o$.

The third problem solved using q-LSKUM code is transonic flow past a hemisphere-cylinder configuration. Figure (9) shows the sketch of the configuration with a section of the grid employed. Mach contours are shown for $M_\infty = 0.7$ and $M_\infty = 1.0$ in figure (10). Figures (11) and (12) show the pressure distribution along the wall and the residue fall for these cases. The experimental values of pressure obtained from AEDC-TR-75-114 are also shown for comparison. The slight disagreement for $M_\infty = 1.0$ case near $x/c = 5$ is typical of measurements near Mach one. For $M_\infty = 0.7$ however, the agreement of computed values with measurements is very good.

Recently, Anandhanarayanan [19] has used LU-SGS method for accelerating q-LSKUM code. Computations for $M_\infty = 2$ flow past a hemisphere on 21^3 grid are very encouraging and a speed-up of about 6 is obtained compared to a purely explicit q-LSKUM code. The q-LSKUM is thus an improvement over the usual LSKUM in terms of accuracy, it can be speeded up using LU-SGS method, and has been applied successfully to a variety of fight vehicles.

REFERENCES

1. Ghosh AK, Robust Least Squares Kinetic Upwind Method for Inviscid Compressible Flows, PhD Thesis, Department of Aerospace Engineering, Indian Institute of Science, Bangalore, 1996.
2. Ghosh AK, Deshpande SM, Least Squares Kinetic Upwind Method for Inviscid Compressible Flows, AIAA Paper 95-1735, 1995.
3. Albone CM, Embedded meshes of controllable quality synthesized from elementary geometric features, AIAA 92-0663, 1992.
4. Ramesh V, Deshpande SM, Euler Computations on Arbitrary Grids using LSKUM, First ICCFD, Kyoto, Japan, July 2000.
5. Deshpande SM, On the Maxwellian Distribution, Symmetric Form and Entropy Conservation for the Euler Equations, NASA TP-2583, 1986.
6. Deshpande SM, Kinetic flux splitting schemes, *Comp. Fluid Dynamics Review*, ed. Hafez M and Oshima K, John Wiley & Sons, 1995.
7. Godlewski E, Raviart P, *Numerical Approximation of Hyperbolic Systems of Conservation Laws*, Springer, 1996.
8. Deshpande SM, Kinetic Theory Based New Upwind Methods for Inviscid Compressible Flows, AIAA paper 86-0275.
9. Mandal JC, Deshpande SM, Kinetic Flux Vector Splitting for Euler Equations, Computers and Fluids, vol 23, No. 2, pp. 447-478, 1994.
10. Deshpande SM, Sekar S, Nagarathinam M, Krishnamurthy R, Sinha PK, Kulkarni PS, 3-Dimensional Upwind Euler Solver Using Kinetic Flux Vector Splitting Method, 13'th ICNMFD, Rome, Italy, 1992.
11. Sekar S, Nagarathinam M, Krishnamurthy R, Kulkarni PS and Deshpande SM, 3-D KFVS Euler Code BHEEMA as Aerodynamic Design and Analysis Tool for Complex Configurations, 14'th ICNMFD, Bangalore, India, 1995.

12. Deshpande SM, Some Recent Developments in Kinetic Schemes based on Least Squares and Entropy Variables, Conference on Solutions of PDE, held in honour of Prof. Roe on the occasion of his 60'th birthday, July 1998, Arcachon, France.
13. Ramesh V, Ghosh AK, Deshpande SM, Computation of Three Dimensional Inviscid Compressible Flows Using Least Squares Kinetic Upwind Method (LSKUM), FM Report, 97 FM 8, Dept. of Aerospace Engg., Indian Institute of Science, Bangalore.
14. Ramesh V, Mathur JS and Deshpande SM, Kinetic Treatment of the Far-Field Boundary Condition, FM Report, 97 FM 2, Dept. of Aerospace Engg., Indian Institute of Science, Bangalore.
15. Ramesh V, Least squares grid-free kinetic upwind method, PhD Thesis, Dept. of Aerospace Engg., Indian Institute of Science, Bangalore, 2001.
16. Taylor GI, The formation of a blast wave by a very intense explosion. Part II: The atomic explosion of 1945, Proc. of Royal Soc. A., 201, pp. 175-186, March 1950.
17. Taylor GI, The formation of a blast wave by a very intense explosion. Part I: Theoretical Discussions, Proc. of Royal Soc. A., 201, pp. 159-174, March 1950.
18. Jernell LS, Aerodynamic loading characteristics of a 1/10 scale model of the three-stage vehicle at Mach numbers from 1.57 to 4.65, NASA TND-1930, Langley Research Center, 1963.
19. Anandhanarayanan K, Nagarathinan M, Deshpande SM, An LU-SGS convergence accelerator for LSKUM based Euler solver, 4'th Annual CFD Symposium of AeSI, Bangalore, 2001.

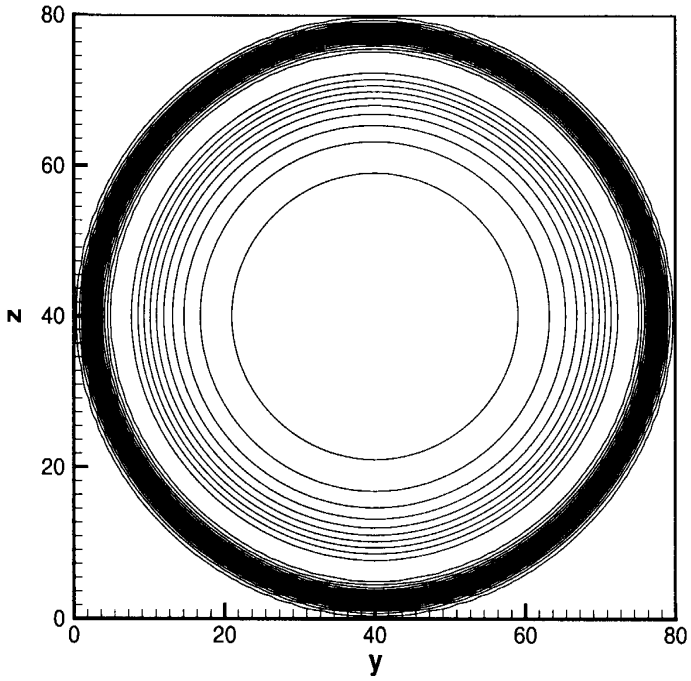

Figure 3. Pressure contours for blast wave problem obtained using LSKUM on a Cartesian grid of 81^3 points.

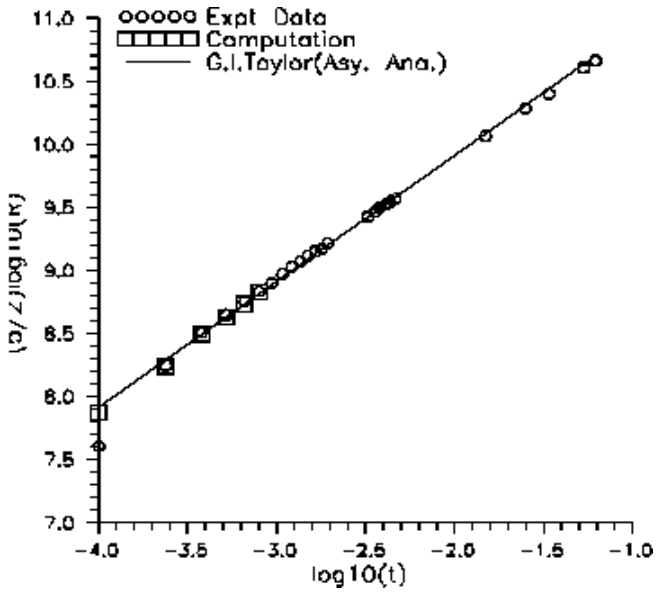

Figure 4. Shock front location for blast wave problem obtained using LSKUM on a Cartesian grid of 81^3 points.

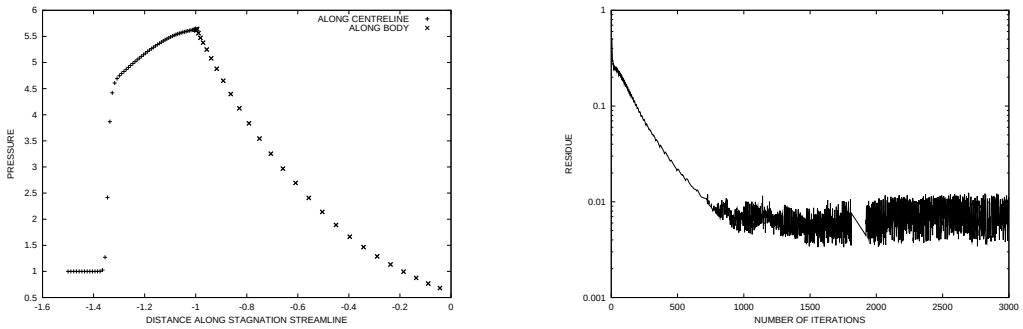

Figure 5. Variation of pressure along the stagnation streamline and convergence history for flow over a hemisphere at $M_\infty = 2$, grid size is 61^3.

Mach Contours

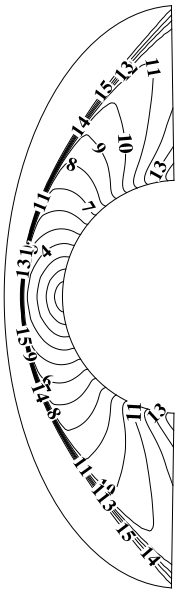

Level	M
15	1.88
14	1.75
13	1.63
12	1.50
11	1.38
10	1.25
9	1.13
8	1.00
7	0.88
6	0.75
5	0.63
4	0.50
3	0.38
2	0.25
1	0.13

Pressure Contours

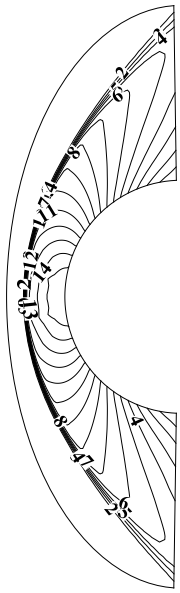

Level	P
15	5.33
14	5.02
13	4.71
12	4.40
11	4.09
10	3.78
9	3.47
8	3.16
7	2.85
6	2.54
5	2.23
4	1.92
3	1.61
2	1.30
1	0.99

Figure 6. Mach and pressure contours for flow over a hemisphere, $M_\infty = 2$, grid $61 \times 61 \times 61$.

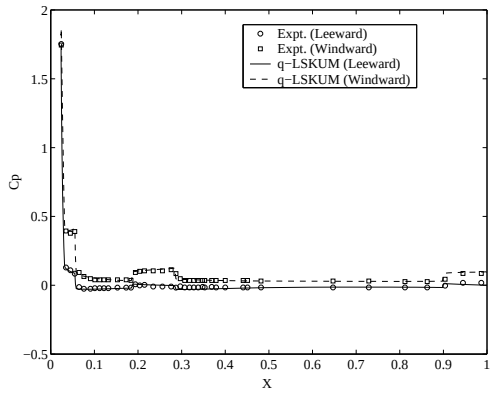

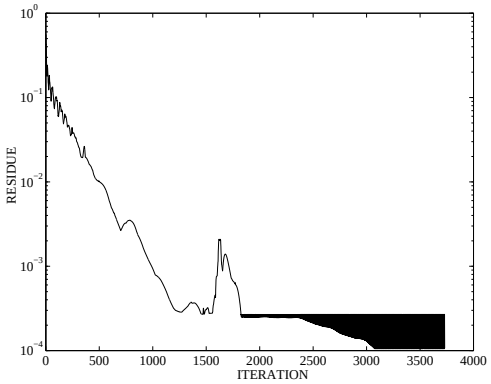

Figure 7. Variation of pressure on the body and convergence history for flow over Scout vehicle configuration, $M_\infty = 4.65$ and $\alpha = 8^o$.

Grid : $81 \times 33 \times 21$

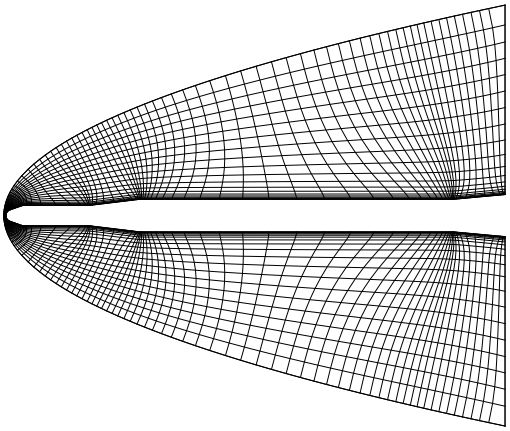

Mach Contours

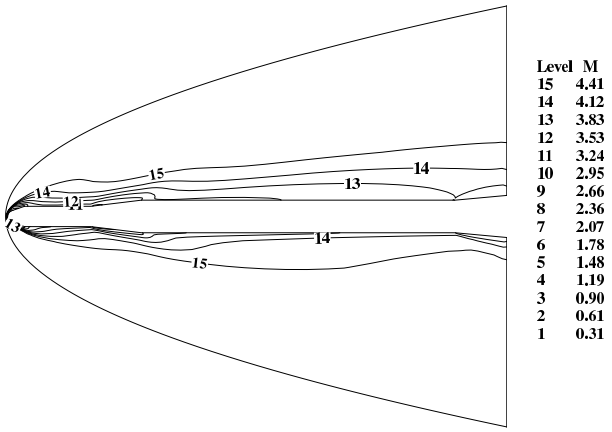

Figure 8. Supersonic flow over Scout vehicle configuration, $M_\infty = 4.65$ and $\alpha = 8^o$.

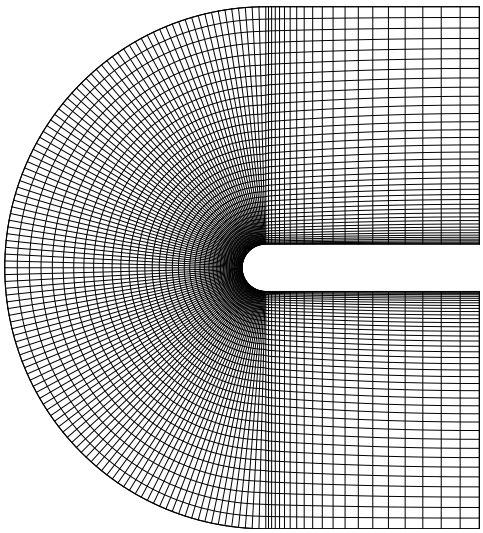

Figure 9. Mesh for hemisphere-cylinder configuration; grid size is $81 \times 41 \times 41$.

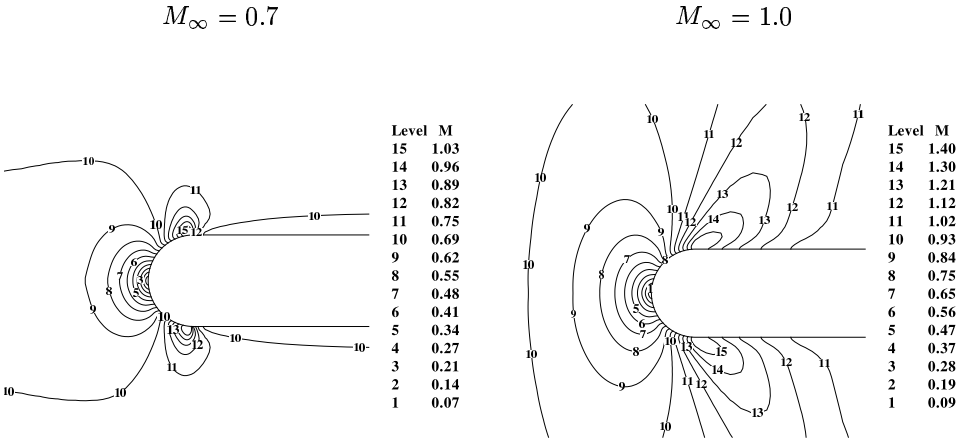

Figure 10. Mach contours for flow over hemisphere-cylinder

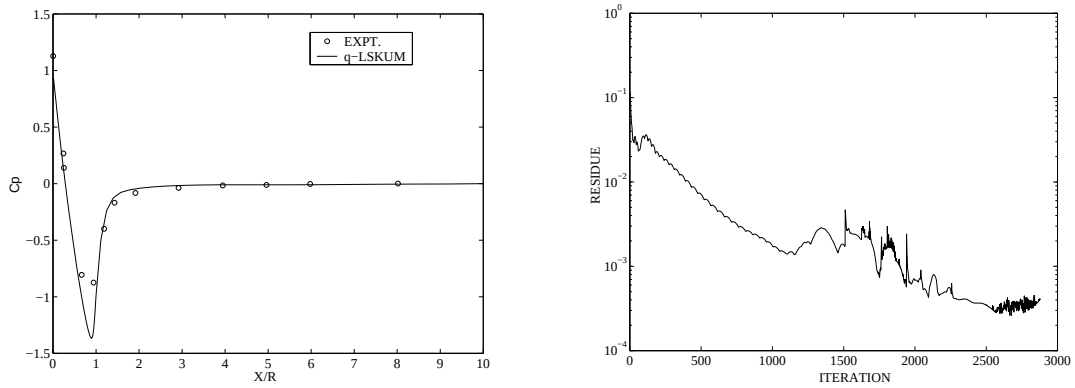

Figure 11. Variation of pressure on the body and convergence history for flow over a hemisphere-cylinder configuration, $M_\infty = 0.7$ and $\alpha = 0^o$.

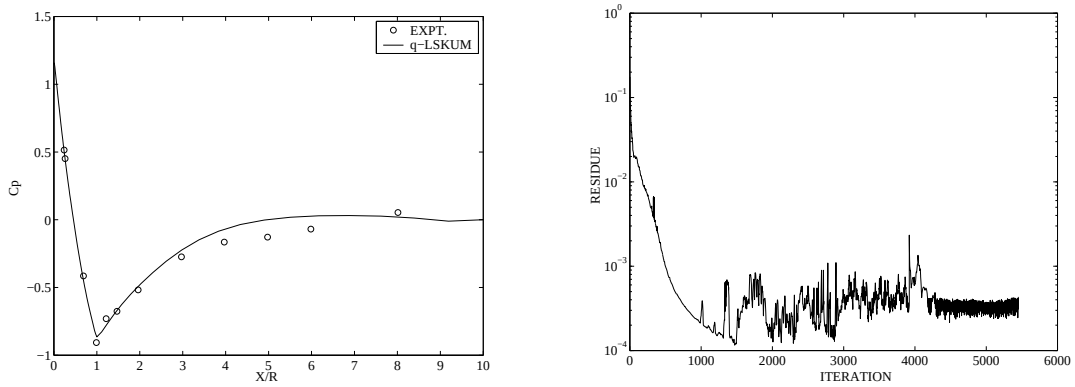

Figure 12. Variation of pressure on the body and convergence history for flow over a hemisphere-cylinder configuration, $M_\infty = 1$ and $\alpha = 0^o$.